Detection of Symmetry Points in Images

Christoph Dalitz, Regina Pohle-Fröhlich and Tobias Bolten

Institute for Pattern Recognition, Niederrhein University of Applied Sciences, Reinarzstr. 49, Krefeld, Germany
{christoph.dalitz, regina.pohle}@hsnr.de, t.bolten@gmail.com

Abstract: This article proposes a new method for detecting symmetry points in images. Like other symmetry detection algorithms, it assigns a "symmetry score" to each image point. Our symmetry measure is only based on scalar products between gradients and is therefore both easy to implement and of low runtime complexity. Moreover, our approach also yields the size of the symmetry region without additional computational effort. As both axial symmetries as well as some rotational symmetries can result in a point symmetry, we propose and evaluate different methods for identifying the rotational symmetries. We evaluate our method on two different test sets of real world images and compare it to several other rotational symmetry detection methods.

1 Introduction

Symmetry can be a useful feature for the identification both of natural objects, like faces (Tao et al., 2009), as well as man-made objects, like vehicles (Kuehnle, 1991). Consequently, algorithms for detecting symmetry points in images have been an area of research for some time (Reisfeld et al., 1995) (Loy and Zelinsky, 2003) (Loy and Eklundh, 2006) (Lee and Liu, 2010). For a survey of symmetry detection algorithms, see (Liu et al., 2009). All of these algorithms assign each image point a "symmetry score" that measures how well the point works as the origin of a mirror operation. The image of symmetry score values can then be considered as a "symmetry transform" of the original image, and symmetry points correspond to maxima in the symmetry transform image.

The symmetry score computation depends on the type of symmetry. The method by Kuehnle (Kuehnle, 1991), e.g., specifically looks for vertical symmetry axes, Reisfeld et al. (Reisfeld et al., 1995) as well as Loy & Eklundh (Loy and Eklundh, 2006) propose different methods for point reflection or rotation symmetry, while Loy & Zelinsky (Loy and Zelinsky, 2003) and Lee & Liu (Lee and Liu, 2010) consider rotational symmetry. The method proposed in the present paper is designed for point reflection symmetry, which is the same as a rotation by π around the mirror point. Let C_n denote the symmetry group of a rotation by an angle $2\pi/n$. Then we are looking for symmetry points of objects with a symmetry group C_{2m}, because, when an object is invariant under a rotation by π/m, it is also invariant under a rotation by π.

A problem in symmetry detection is that the size of the symmetric object is generally not known beforehand. For computing the symmetry score value however, ideally only pixels belonging to the object should be considered. The symmetry transform by Reisfeld et al. (Reisfeld et al., 1995) requires an input parameter that suppresses distant pixels exponentially, which sidesteps the problem by letting the user guess an object radius. The method by Lee & Liu (Lee and Liu, 2010) tries a whole range of radii, but this adds even more computational complexity to an already very complex method. As a workaround, they suggest the use of image pyramids so that only regions that seem promising in low resolutions are examined in full detail. Our method in the present paper offers a different solution via a recursion formula that connects the score value for radius $r+1$ with the score value for radius r, which reduces the computational overhead of trying different radii considerably.

Another problem for the detection of rotational symmetric objects is that, depending on the view point, the symmetry can be "skewed" (Kanade, 1981) (see Fig. 1(a)). Lee & Liu address this problem with a frieze expansion around each potential rotation center (Lee and Liu, 2010). A simpler approach with considerably less computational cost can be based on the observation that a C_{2m} symmetry *approximately* becomes a point reflection (C_2) symmetry, provided the object does not extend too much in the direction perpendicular to the image plane. In practice, rotational symmetry will therefore generally show up as a C_2
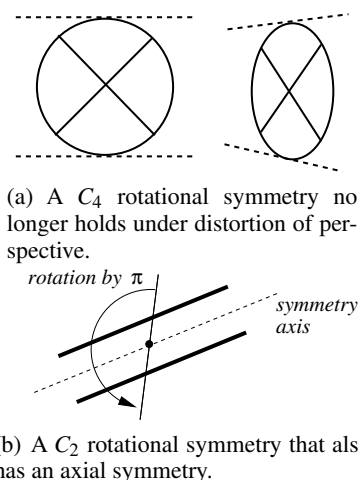
(a) A C_4 rotational symmetry no longer holds under distortion of perspective.

(b) A C_2 rotational symmetry that also has an axial symmetry.

Figure 1: The problems of "skewed symmetry" and axial symmetry in rotational symmetry detection.

symmetry, for which our method is specifically designed.

It should be noted however, that some pure axial symmetries also show up as C_2 symmetries. A particularly frequent case are parallel lines (see Fig. 1(b)). When detecting rotational symmetry through point reflection symmetries, it is thus necessary to distinguish the actual rotation symmetries from pure axial symmetries. In this paper we will investigate different criteria for making this discrimination.

This paper is organized as follows: Sec. 2 describes the computation of our symmetry score value and the determination of the symmetry radius. Sec. 3 describes different possible features useful for distinguishing high score points belonging to a rotational symmetry from those belonging to an axial symmetry. Sec. 4 evaluates these features on a dataset of real world images. Moreover, the resulting symmetry detection is compared on two different data sets to the classic method by Reisfeld et al. (Reisfeld et al., 1995) (Reisfeld et al., 1990) and to the newer method by Loy & Eklundh (Loy and Eklundh, 2006), which was reported as the best method in (Park et al., 2008) and (Rauschert et al., 2011). In the final Sec. 5, we discuss open questions and make suggestions for further research.

The source code of our symmetry transform and the test data set with ground truth information will be made available on the authors' website[1].
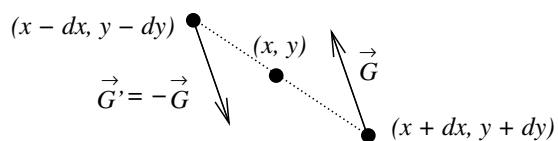
Figure 2: Point reflection of an image at point (x,y) maps the gradient $\vec{G}$ at $(x+dx,y+dy)$ onto the gradient $\vec{G}'$ at $(x-dx,y-dy)$.

2 The symmetry detection method

The general approach to symmetry detection consists in first computing a measure for the symmetry of each point, and then selecting points with a high symmetry score. In this section, we define a measure for point symmetry and show how this measure cannot only be utilized for detecting symmetry points, but also the size of the symmetry region.

2.1 The symmetry measure

Like Reisfeld et al. (Reisfeld et al., 1995), we utilize the gradient image rather than the original image, because we do not want homogeneous regions to be recognized as symmetric. The gradient image can be computed from a greyscale image with a Sobel filter (Gonzalez and Woods, 2002). Let us denote the gradient image with $\vec{G}(x,y)$. When an image is mirrored at point (x,y), the gradient $\vec{G}(x+dx,y+dy)$ becomes $-\vec{G}(x-dx,y-dy)$ (see Fig. 2). We conclude that one necessary condition for symmetry around point (x,y) is that these two gradients point in opposite directions, or that their scalar product $\langle \cdot, \cdot \rangle$ is negative:

$$\left\langle \vec{G}(x+dx,y+dy), \vec{G}(x-dx,y-dy) \right\rangle < 0 \quad (1)$$

This scalar product takes a minimum when the two gradients are anti parallel. We therefore define as a measure for the symmetry around point (x,y)

$$S(x,y,r) = -\sum_{dy=1}^{r} \sum_{dx=-r}^{r} \ldots$$
$$\left\langle \vec{G}(x+dx,y+dy), \vec{G}(x-dx,y-dy) \right\rangle$$
$$-\sum_{dx=1}^{r} \left\langle \vec{G}(x+dx,y), \vec{G}(x-dx,y) \right\rangle \quad (2)$$

where r is the radius of the symmetry region. The sum omits the negative values $dy < 0$ because these are already taken into account by the mirror operation in the argument of the gradient. The symmetry point (x,y) itself is completely omitted in the sum. The minus sign is added for convenience so that S is larger for higher symmetry, not vice versa.

It should be noted that the measure (2) does not only take into account the gradient directions, but also their absolute strength. This has the effect that symmetric regions with strong edges have a higher symmetry measure than regions with weaker edges, but otherwise the same symmetry. One way to smooth out this difference is by transforming the gradient strength as suggested by Reisfeld et al. (Reisfeld et al., 1995):

$$\vec{H} = \frac{\vec{G}}{\|\vec{G}\|} \cdot \log(1 + \|\vec{G}\|) \qquad (3)$$

and then applying (2) to $\vec{H}$ instead of $\vec{G}$. Instead of $\log(1+x)$, any other monotonous transformation could be used, of course. It is an open question however, whether such a rescaling actually improves the detection of symmetry points. The experiments described in Sec. 4 have therefore been done both with transformed and untransformed gradients.

2.2 The size of the symmetry region

When the symmetry measure $S(x,y,r)$ according to (2) is evaluated for different values of r, this provides a way to automatically determine the size of the symmetry region around (x,y). Unlike the symmetry measure by Reisfeld et al., (2) does not include an exponential damping factor depending on a predefined region size. This means that, for a given point (x,y), the values $S(x,y,r)$ can be subsequently computed for $r = 1, 2, \ldots, r_{max}$ without any additional computational effort, simply by reordering the sum (2) to

$$
\begin{aligned}
S(x,y,r) = {}& S(x,y,r-1) \\
& - \sum_{dx=-r}^{r} \left\langle \vec{G}(x+dx,y+r), \vec{G}(x-dx,y-r) \right\rangle \\
& - \sum_{dy=-r+1}^{r-1} \left\langle \vec{G}(x+r,y+dy), \vec{G}(x-r,y-dy) \right\rangle \quad (4)
\end{aligned}
$$

The symmetry value $S(x,y)$ and region radius $R(x,y)$ for a point (x,y) can then be defined as

$$
\begin{aligned}
R(x,y) &= \operatorname{argmax}\{S(x,y,r) \,|\, r = 1, \ldots, r_{max}\} \\
\text{and} \quad S(x,y) &= S(x,y,R) \qquad (5)
\end{aligned}
$$

When the region radius is close to r_{max}, larger values for r could also be tried to find the next local maximum of S. This can save some computing time because large radii are then only investigated at "promising" points.

2.3 Runtime complexity

For an image with n pixels, the Sobel filter requires $9n$ additions and n multiplications and is thus an $O(n)$

algorithm. The symmetry transform requires $r_{max}^2/2$ multiplications and additions for each pixel. As both operations are done subsequently, the total runtime of our symmetry transform is $O(r_{max}^2 \cdot n)$. Even though this is in O-Notation the same runtime complexity as for the symmetry transform by Reisfeld et al., our transform is considerably faster, because it only requires algebraic operations and no exponential and trigonometric functions. Loy & Eklundh did not estimate the runtime complexity of their algorithm in (Loy and Eklundh, 2006). As their algorithm does not take all image pixels as input, but only the much smaller set of SIFT feature points (Lowe, 2004), the runtime complexity depends on two factors: the runtime complexity of the SIFT extraction, and the number of SIFT points returned, which depend very much on the image content, thereby making a worst case runtime estimation difficult.

On an Intel P8400 2.26 GHz CPU and with $r_{max} = 50$, our algorithm took constantly 0.2 sec on a 200×150 image from the CVPR 2011 dataset and 2.7 sec on a 600×400 image from our dataset, while an optimized implementation (exponentials replaced with lookup tables) of Reisfeld's transform took about 9 sec (200×150, $\sigma = 25$) and 250 sec (600×400, $\sigma = 25$), respectively. The runtime of Loy & Eklundh's algorithm varied considerably over the images and was between 0.3 and 1.0 sec on a 200×150 image, and between 1 and 18 sec on a 600×400 image.

3 Rotational versus axial symmetry

As can be seen in Fig. 3, the symmetry transform described in Sec. 2 assigns high score values to centers of point symmetry. Some of these belong to rotational symmetries, while others belong to axial symmetries, mostly due to parallel strong edge lines. To discriminate between these types of symmetry, we observe that, for an axial symmetry, we obtain other symmetry points when moving from one symmetry point along the symmetry axis. The same does not hold for a purely rotational symmetry. This means that axial symmetries result in line shaped regions of high symmetry scores, while rotational symmetries lead to more circularly shaped regions of high symmetry. We have therefore implemented the following three features for determining the symmetry type of a given candidate point (x,y):

Edge directedness, computed on the gradient of the symmetry transform. This measures how "strongly directed" the edges of the symmetry transform are. The feature is the maximum rel-

Figure 3: Symmetry transform according to Eqs. (4) and (5) of the image on the left.

ative frequency in a histogram of the edge directions, weighted by the gradient absolute value, in a $k \times k$ window around point (x, y). Natural choices for the number of bins in the direction histogram are 8 or 16. The "edge directedness" should be higher for axial symmetries.

Covariance eigenratio, computed on the symmetry transform image. We compute the covariance matrix $\mathbf{K}$ for the points in a $k \times k$ window around (x, y) as

$$\mathbf{K} = \frac{1}{N} \sum_{dx=-k/2}^{k/2} \sum_{dy=-k/2}^{k/2} S(x+dx, y+dy) \\ \times \begin{pmatrix} dx\,dx & dx\,dy \\ dy\,dx & dy\,dy \end{pmatrix} \quad (6)$$

where $S(x, y)$ is the symmetry transform value at (x, y), and the normalization factor N is the sum over all symmetry values in the window. The eigenvalues of $\mathbf{K}$ indicate how strongly the values spread in the direction of the corresponding eigenvector. Consequently, the ratio between the smaller and the larger eigenvalue should be higher for rotational symmetry, which are more isotropically spread around (x, y).

Antiparallel directions, computed on the gradient of the original greyscale image. We compute the direction histogram of all gradients in a window with the symmetry radius $R(x, y)$ according to Eq. (5). Only those gradients are taken into account for which the mirrored gradient is "antiparallel", i.e. the cosine of the angles between the gradients is less than -0.975. The feature is the highest relative frequency in the direction histogram. Again the number of histogram bins can be 8 or 16. The value for "antiparallel directions" should be lower for rotational symmetries.

In our experiments, described in Sec. 4.1, the feature *edge directedness* with 16 histogram bins showed the best performance.

4 Experimental results

For testing symmetry detection, there are currently not many data sets available. Park et al. (Park et al., 2008) selected images from different object recognition datasets for the CVPR 2008 conference, but the resulting dataset is no longer available. At the CVPR 2011 conference, there was a workshop on symmetry detection, and the data set, consisting of 42 images, used for evaluation is still available (Rauschert et al., 2011). As using this data set allowed us to compare our method to the other methods evaluated in this workshop, we have used this as one of our test sets.

To allow for a more detailed investigation both of our method and for future research, we have additionally created a new larger test set and ground truth data. The new data set consists of 159 images of size 600×400, containing 27 different subjects. Each subject is shown in different perspectives and both in context and in detail. The detail images can be useful because, in the contextual images, the environment often shows additional incidental symmetries. Like Park et al. (Park et al., 2008), we have only labelled those C_{2m} symmetries that are "visually obvious dominant symmetries" according to human observers. In the ground truth meta data, we have labelled the symmetry points and the radius of the symmetric region.

We have used these images both for an evaluation of the rotational symmetry detection, and for an evaluation of the symmetry type discrimination. For the latter we have created different ground truth data and a different set of test points.

4.1 Evaluation of symmetry type discrimination

To evaluate the three features described in Sec. 3 for discriminating between rotational and axial symmetry points, we have selected the ten highest local maxima in the symmetry transform of each image from our own test set, and labeled these points manually as be-
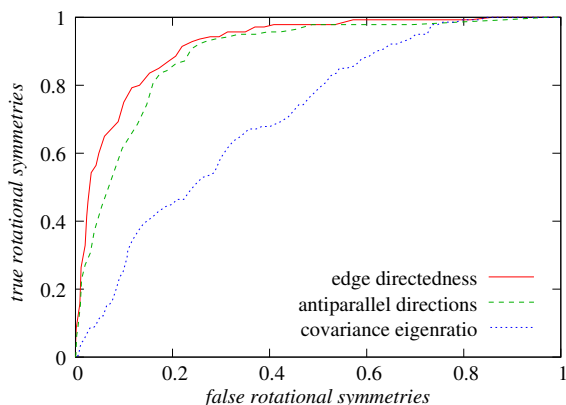
Figure 4: ROC curve comparing the performance of the three features for discriminating between rotational and axial symmetry. "False rotational symmetries" denotes the rate of the axial symmetries erroneously classified as rotational symmetries, and "true rotational symmetries" the rate of the correctly classified rotational symmetries.

longing to an axial or rotational symmetry. After an omission of unclear cases, these provided a test set of 1346 symmetry points, of which 140 belonged to rotational symmetry.

For each feature, the classification is based on a threshold on the feature value. By comparing the rates of correctly and erroneously detected rotational symmetries for different thresholds, we can thus compare the discriminating power of the three features. For the $k \times k$ windows, we have used $k = 7$, and as numbers of histogram bins we have tested 8 and 16. In the case of "edge directedness", 16 bins were better, and for "antiparallel directions", 8 bins were better, i.e. had a higher area under the ROC curve (AUC). The ROC curves in Fig. 4 show that "edge directedness" performed best on our test data. Even though the feature "antiparallel directions" has a clearly larger AUC than "covariance eigenratio", it is still slightly lower than that of "edge directedness". As "edge directedness" has the additional advantage of being faster to compute due to the smaller window size, we have used this feature for sorting out the axial symmetries. The values in the upper left corner of the ROC curve correspond to thresholds between 0.23 and 0.29 for the "edge directedness", so that we have chosen a threshold of 0.27 as the criterion for rotational/axial symmetry discrimination in Sec. 4.2.

4.2 Evaluation of rotational symmetry detection

To compare a new method with other methods for rotational symmetry detection, there are principally two

approaches: one is to implement and run the different algorithms on a new test set, the other one is to run the new algorithm on an older data set for which results have already been reported in an earlier study. For the latter approach, we have used the CVPR 2011 data set (Rauschert et al., 2011). For the former approach, we have deployed the code published by Loy & Eklundh on their website (Loy and Eklundh, 2006), and have additionally implemented ourselves the classic method by Reisfeld et al. (Reisfeld et al., 1995).

Concerning the latter algorithm, it should be noted that Reisfeld at al. gave different formulas for the rotational symmetry score in (Reisfeld et al., 1990) and (Reisfeld et al., 1995). We have implemented both to allow for a comparison between these formulas. In both of Reisfeld's symmetry measures, contributions by a point $\vec{p}$ with mirror point $\vec{p}'$ are weighted with a factor $\exp(-\|\vec{p} - \vec{p}'\|/2\sigma)$, which suppresses contributions of points far away from the symmetry center. Reisfeld et al. made no suggestion how to choose the parameter σ, which must be related to the radius r of the symmetric objects to be looked for[2]. We have used the relation $r = 2\sigma$ and, for performance reasons, have cut off contributions of points at a distance greater than 3σ. As our ground truth data contained the actual object radius r, we have used this radius as the input parameter for each particular image.

To see whether a logarithmic gradient transformation actually has the positive effect conjectured by Reisfeld et al., we have created their and our symmetry transform both on the raw gradient image and on the gradient image that has been transformed according to Eq. (3). In addition to the method by Loy & Eklundh, this resulted in a total of seven different algorithms that we could run on our test data.

All of these symmetry transforms do not uniquely yield symmetry points, but only symmetry scores (or "votes") for which there is no absolute criterion whether a score actually represents a symmetry or not. To avoid the introduction of a threshold on the symmetry score that is to a certain degree arbitrary, we have therefore evaluated the symmetry detection on basis of the highest symmetry score in the image. For the methods by Reisfeld at al. and Loy & Eklundh, the highest score value in the image should represent

---

[2] The impact of the choice of σ in relation to the object size would have been an interesting subject of investigation in itself, that was however beyond the scope of the present study. We settled on $r = 2\sigma$ with the following reasoning:

The weight given to all pixels of an object with radius r in Reisfeld's et al. symmetry score is proportional to $2\pi \int_0^r s e^{-s/\sigma} ds = 2\pi\sigma^2 (1 - (1 + r/\sigma) e^{-r/\sigma})$. Setting $r = 2\sigma$ results in a weight of 60% for the object; smaller values for σ increase this ratio, but would suppress contributions from near the object contour too much.
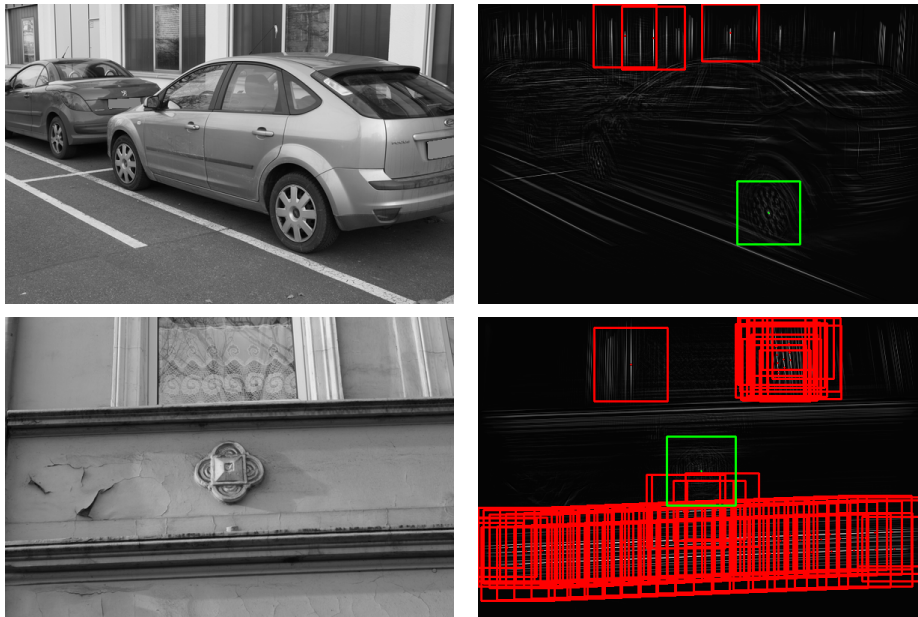
Figure 5: Some input images (left) and the corresponding symmetry transforms and detected symmetry points highlighted in green (right). The red points are local maxima with a higher symmetry score that have been rejected due to a too high "edge directedness".

the dominant rotational symmetry. In the case of our method, we have sorted out the axial symmetries with the following algorithm:

1. Find all local maxima in the symmetry transform and sort them by their score value in descending order.

2. Find the highest score value in this list that has an "edge directedness" less than 0.27, which is an indicator for a rotational symmetry instead of an axial symmetry, according to the results of Sec. 4.1.

Fig. 5 shows for sample images from our test set both the resulting highest score and the higher scores that have been sorted out by the second criterion.

Results on the CVPR 2011 data set. The CVPR 2011 data set was used at the workshop on symmetry detection at CVPR 2011 for comparing two yet unpublished algorithms by Kim & Lee & Chee and by Kondra & Petrosino with the algorithm by Loy & Eklundh (Loy and Eklundh, 2006) . It consists of 42 images (including 4 doublets) of a size about 200×150 that had been harvested on the Internet; it includes ground truth data of the symmetry centers and the axes length of the elliptic symmetry regions.

In the experiments reported in (Rauschert et al., 2011), the algorithms returned more than one symmetry point per image and Rauschert et al. reported both a recall and a precision value. As we only take into account the highest symmetry count, we can only mea-
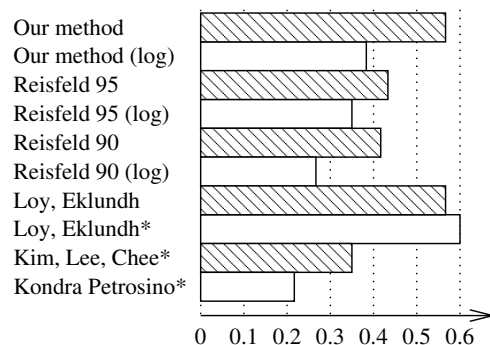

Figure 6: Recognition rates of the tested algorithms on the CVPR 2011 data set. Values with an asterisk are the precision values reported in (Rauschert et al., 2011).

sure the recognition rate as a precision value, i.e. the number of returned symmetry points that actually correspond to a ground truth symmetry. We have considered a symmetry to be found when the detected symmetry point had a distance less than 5 pixels from a ground truth symmetry center.

The measured values for our algorithm and the algorithm by Reisfeld et al. together with the results reported in (Rauschert et al., 2011) can be seen in Fig. 6. As our recognition rate is computed slightly different from the precision value by Rauschert et al., we have given both values for the algorithm by Loy & Eklundh, which shows that both rates are compara-

582

	Count	Our method		Reisfeld 95		Reisfeld 90		Loy & Eklundh
		grad	*log*	*grad*	*log*	*grad*	*log*	
Detail	83	0.60	0.53	0.33	0.22	0.41	0.40	0.37
Context	76	0.33	0.39	0.18	0.20	0.37	0.36	0.37
Front	43	0.70	0.63	0.42	0.30	0.53	0.49	0.70
Light skew	57	0.58	0.53	0.25	0.14	0.47	0.40	0.39
Strong skew	59	0.20	0.29	0.15	0.20	0.20	0.27	0.12
Total	159	0.47	0.47	0.26	0.21	0.39	0.38	0.37

Table 1: Symmetry recognition rates on our test set for the different algorithms on different image categories ("Detail" etc.). "grad" means that the gradient image has been used, while "log" means that the gradients have been transformed according to Eq. (3).

ble observables. The results show that our method is comparable to the best method from the CVPR 2011 workshop. A closer look at the individual images showed that our algorithm performed best on the 15 images with C_∞ symmetries (0.73 versus 0.60 by Loy & Eklundh), which is easily understandable as the discrete C_n symmetries also include some odd n, for which our algorithm is less suited. Due to the small number of images, this difference in the recognition rate is however of limited significance. It is interesting to observe that a gradient transformation according to Eq. (3) did not improve the symmetry detection, but deteriorated the total recognition rate slightly. A possible explanation can be that this transformation amplifies background and noise edges, as can be seen in Fig. 7.

Results on our own data set. To test the robustness of the algorithms with respect to skew and background noise on a larger data base, we have additionally run the algorithms on our own data set. Due to the larger image size, we have here considered a symmetry point as correctly detected when the resulting point had a distance less than 10 pixels from a ground truth symmetry point.

The recognition rates of correctly detected symmetry points in Tbl. 1 show, somewhat surprisingly, that the later 1995 method by Reisfeld et al. performed poorer than their 1990 method, a difference that was even significant for a significance level of 5% according to McNemar's test (Diettrich, 1998). Our new method was better than the 1990 method by Reisfeld. Again, the gradient transformation according

(a) Gradient absolute values.

(b) Gradient absolute values after applying Eq. (3).

(c) Symmetry transform based on (a).
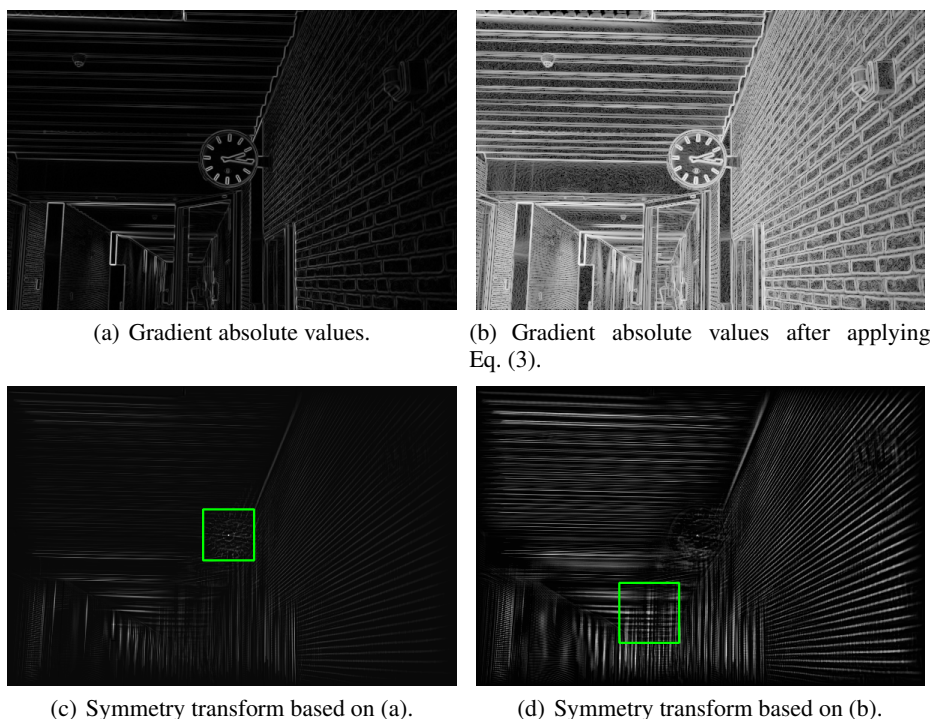

(d) Symmetry transform based on (b).

Figure 7: Effect of the logarithmic gradient transformation according to Eq. (3) on a sample image from our own data set. The detected symmetries by our algorithm are highlighted in green.
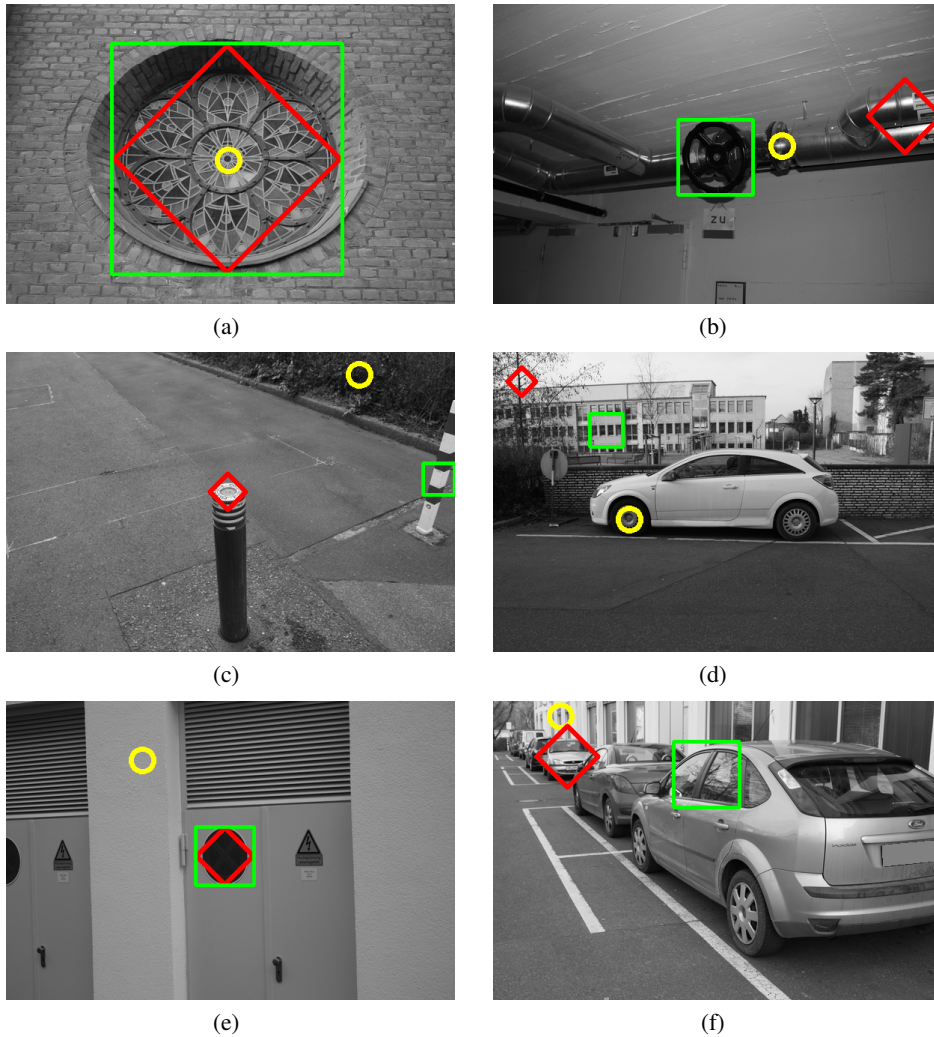
Figure 8: Some input images and the detected dominant rotational symmetry by our algorithm (green squares), and the algorithms by Reisfeld et al. 1990 (red diamonds) and Loy & Eklundh (yellow circles).

to Eq. (3) deteriorated the symmetry detection. As the deteriorating effect can be observed on both different tested data sets, we conclude that the logarithmic normalization of the gradient cannot be recommended for symmetry detection.

Of all tested algorithms, the new method performed on average even better than the algorithm by Loy & Eklundh, which had shown the best performance in the studies (Park et al., 2008) and (Rauschert et al., 2011). As the varying results for the categories front/skewed show, the recognition rates of all algorithms are lower for skewed rotation symmetries. The algorithm by Loy & Eklundh is most susceptible to distortion due to perspective: for unskewed symmetries it shows the same performance as our algorithm, but with skew the recognition rates become even lower than those of the algorithm by Reisfeld et al.. This is presumably due to the fact that a rotational symmetry no longer holds in this case, but approximately becomes a C_2 mirror symmetry, which is still detected by our method. Under stronger skew, this approximation no longer holds and our method also fails to detect most symmetries.

Fig. 8 shows exemplary results of all three algorithms on images from our data set. There were a number of images on which all three algorithms worked well (like 8(a)), as well as images on which all algorithms failed (e.g. due to a too strong skew like in 8(f)). Neither algorithm was however consistently better than a different algorithm on all images: for each algorithm, there were images on which it was the only one that detected a symmetry (see 8(b)-8(d)).

5 Conclusions

The new symmetry transform proposed in this paper is very easy to implement and has shown a symmetry detection rate that was both better than the algorithm by Loy & Eklundh and than the symmetry transform by Reisfeld et al. Even though the qualitative runtime complexity of $O(nr^2)$ is similar to the latter algorithm, with n the number of image pixels and r the maximum radius, the absolute runtime of the new method is lower because the symmetry score computation only involves scalar products. While the method primarily computes a point reflection symmetry (C_2 symmetry) score, these can be discriminated into axial and rotation symmetries with a criterion for the "edge directedness" in the symmetry transform around the symmetry point.

For the method by Reisfeld et al., our experiments have shown interesting results: first that the rotational symmetry score *RS* proposed in their later paper (Reisfeld et al., 1995) performed worse than the score *CS* from their earlier paper (Reisfeld et al., 1990). Moreover, the logarithmic transformation of the gradients did not have the positive effect that Reisfeld at al. have conjectured, which leads to the question whether other transformations might be helpful. Together with the question of an optimal choice for the parameter σ, these are interesting points that require more detailed investigations.

For the new symmetry transform, there are also a number of interesting open questions for future research. One is the evaluation and optimization of the automatic radius detection. Others are the extension of the radius detection to rectangular symmetric regions, or the effect of other gradient transformations. Another important question for every kind of symmetry transform is what *absolute* criteria actually determine a symmetry point, a problem that we have circumvented in the present study by using the *relative* criterion of the highest score in the image.

It should be noted that the application of the new symmetry transform is not necessarily restricted to symmetry detection. It may also be a useful starting point for feature extraction from images.

REFERENCES

Diettrich, T. (1998). Approximate statistical tests for comparing supervised classification learning algorithms. *Neural Computation*, 10:1895–1923.

Gonzalez, R. and Woods, R. (2002). *Digital Image Processing*. Prentice-Hall, New Jersey, 2nd edition.

Kanade, T. (1981). Recovery of the three-dimensional shape of an object from a single view. *Artificial Intellgence*, 17:409–460.

Kuehnle, A. (1991). Symmetry-based recognition of vehicle rears. *Pattern recognition Letters*, 12:249–258.

Lee, S. and Liu, Y. (2010). Skewed rotation symmetry group detection. *IEEE Transactions on Pattern Analysis and Machine Intelligence*, 32(2):1659–1671.

Liu, Y., Hel-Or, H., Kaplan, C., and Gool, L. V. (2009). Computational symmetry in computer vision and computer graphics. *Foundations and Trends in Computer Graphics and Vision*, 5:1–195.

Lowe, D. (2004). Distinctive image features from scale-invariant keypoints. *International Journal of Computer Vision*, 10(2):91–110.

Loy, G. and Eklundh, J. (2006). Detecting symmetry and symmetric constellations of features. In *European Conference on Computer Vision (ECCV)*, pages 508–521.

Loy, G. and Zelinsky, A. (2003). Fast radial symmetry for detecting points of interest. *IEEE Transactions on Pattern Analysis and Machine Intelligence*, 25(8):959–973.

Park, M., Lee, S., Chen, P., Kashyap, S., Butt, A., and Liu, Y. (2008). Performance evaluation of state-of-the-art discrete symmetry detection algorithms. In *IEEE Conference on Computer Vision and Pattern Recognition (CVPR)*, pages 1–8.

Rauschert, I., Brockelhurst, K., Liu, J., Kashyap, S., and Liu, Y. (2011). Workshop on symmetry detection from real world images - a summary. In *IEEE Conference on Computer Vision and Pattern Recognition (CVPR)*.

Reisfeld, D., Wolfson, H., and Yeshururn, Y. (1990). Detection of interest points using symmetry. In *3rd International Conference on Computer Vision*, pages 62–65.

Reisfeld, D., Wolfson, H., and Yeshururn, Y. (1995). Context-free attentual operators: The generalized symmetry transform. *International Journal of Computer Vision*, 14:119–130.

Tao, C., Shanxua, D., Fangrui, L., and Ting, R. (2009). Face and facial feature localization based on color segmentation and symmetry transform. In *International Conference on Multimedia Information Networking and Security (MINES)*, pages 185–189.